Separation Science and Technology
Publication details, including instructions for authors and subscription information:
http://www.informaworld.com/smpp/title~content=t713708471

Increasing Filtrate Flux of Cross-Flow Filtration with Side Stream

Rome-Ming Wu[ab]; Kuo-Jen Li[a]
[a] Department of Chemical and Materials Engineering, Tamkang University, Tamsui, Taipei County, Taiwan [b] Energy and Opto-Electronic Materials Research Center, Tamkang University, Tamsui, Taipei County, Taiwan

Online publication date: 23 April 2010

To cite this Article Wu, Rome-Ming and Li, Kuo-Jen(2010) 'Increasing Filtrate Flux of Cross-Flow Filtration with Side Stream', Separation Science and Technology, 45: 7, 975 — 981
To link to this Article: DOI: 10.1080/01496391003666973
URL: http://dx.doi.org/10.1080/01496391003666973

Separation Science and Technology, 45: 975–981, 2010

ISSN: 0149-6395 print/1520-5754 online
DOI: 10.1080/01496391003666973

Taylor & Francis
Taylor & Francis Group

Increasing Filtrate Flux of Cross-Flow Filtration with Side Stream

Rome-Ming Wu[1,2] and Kuo-Jen Li[1]
[1]*Department of Chemical and Materials Engineering, Tamkang University, Tamsui, Taipei County, Taiwan*
[2]*Energy and Opto-Electronic Materials Research Center, Tamkang University, Tamsui, Taipei County, Taiwan*

In this study, we use simulations to calculate the velocity fields of cross-flow filtration, overall filtration resistance, and shear force distribution on the membrane surface and then compare the results with experimental results. Also, side stream ideas are used in this study in hopes of changing the flow strength conditions in the filtration chamber to increase shear force on the membrane surface under identical energy loss in order to achieve the effect of increasing filtrate flux. The simulation and experimental results show that this cross-flow filtration with side stream can effectively increase the filtrate flux and lengthen the fouling time.

Keywords CFD; cross-flow; filtrate flux; shear force; side stream

INTRODUCTION

Cross-flow filtration is fairly widely used in many solid–liquid separation industry technologies (1–3). It is already known that, in cross-flow filtration, the hydraulic force applied to the membrane surface is a key factor in impacting filter cake patterns and overall filtration resistance. Under broad operative conditions, the filtrate flux generally increases along with increases in cross-flow speed and filtration pressure differential. However, excessively high cross-flow speed and filtration pressure differential can also lead to increased costs and energy loss.

In the membrane filtration process, the resistance caused by the filter cake has an essential impact on filtration effects. As a result, the means of reducing the production of filter cakes and thus a reduction in filtration resistance to effectively increase filtrate flux is an important issue in membrane filtration (4–6). In the solid–liquid separation process, changes in fluid dynamics in the filtration chamber have a substantial impact on the filtration effect. Consequently, many scholars have researched and analyzed changes in fluid dynamics (7–11). Berman (12) first used laminar flow to determine the flow of fluids in two porous medium plates. Deen (13) used the fluid dynamics perspective to widely research and analyze the movement of particles in pores. Drew et al. (14) found the connection between the fluid dynamics effects of small suspended spheres under laminar flow conditions and under fast flowing conditions in the conveyor tubes of porous boundaries. Hwang et al. (15) presented a force balance model for force between fluid dynamics and particles in order to explain the force impact of particles on filter surfaces. Bowen and Sharif (16) explained the significant impacts between powder and fluid dynamics when particles are larger than pores and explained full blockage models in pores. Consequently, they suggested the use of membranes with higher surface potential.

Many researchers have attempted to alter the dynamics in filtration chambers, and these studies have been found to indeed have an effect on filtrate flux. Gupta et al. (17) applied a spiral baffle to cross-flow filtration and found that doing so could increase filtrate flux by 50%. Millward et al. (18) placed obstacles that increased turbulence around the membrane to increase filtrate flux. Ma et al. (19) combined impulse reverse wash and surface modification technologies, obtaining superior filtrate flux under low suspension concentration and short operation. Kuberkar and Davis (20) compared the differences in the cross-flow filtration and reverse-wash and pointed out that cross-flow filtration can reduce the rate at which external caking occurs, while the reverse-wash has comparatively better treatment effects for internal fouling.

In addition, in a study on shear force, Hoek et al. (21) explained that increasing shear stress can reduce membrane caking when membrane pore channel heights are fixed through deriving connections between membrane geometric structure, shear force size, and caking speed of RO and NF. Under a fixed flow, increasing shear force

Received 1 November 2009; accepted 31 December 2009.
Address correspondence to Rome-Ming Wu, Department of Chemical and Materials Engineering, Tamkang University, 151 Ying-Chuan Road, Tamsui, Taipei County 25137, Taiwan. Fax: +886-2-26209887. E-mail: romeman@mail.tku.edu.tw

can reduce membrane caking; under fixed shear force, the membrane pore height does not have a great impact on caking.

CFD has been widely applied in many applications, like porous medium (22), drinking water treatment (23), sedimentation (24), hydrocyclone separation (25–26), etc. This study will perform an experiment in introducing a side stream to increase the membrane shear force to slow the cake formation and increase the filtrate flux. CFD will also be used to calculate the distribution of the membrane shear force. The numerical solutions were carried out using commercial CFD code FLUENT 6.1.

EXPERIMENTAL MATERIALS AND METHODS

The powder used in this experiment is ploymethyl methacrylate (PMMA), produced by Japan's Soken Chemical & Engineering Co., Ltd. The powder appears as a white powder. Observation using a scanning electron microscope shows that the shape of the powder bodies is almost that of a sphere. The particle diameter of the powder is 0.8 μm; the moisture content is 0.5%; the particle density is $1190\,kg/m^3$.

The filter membrane used in filtration was produced by ADVANTEC MFS, Inc. The material is mixed cellulose ester; the filter is a hydrophilic membrane with a maximum operating temperature of 55°C, an average pore diameter of 0.1 μm, a porosity of 74%, and a thickness of 125 μm.

Figure 1 depicts a diagram of the basic filtration system. The suspension fluid is prepared prior to the experiment.

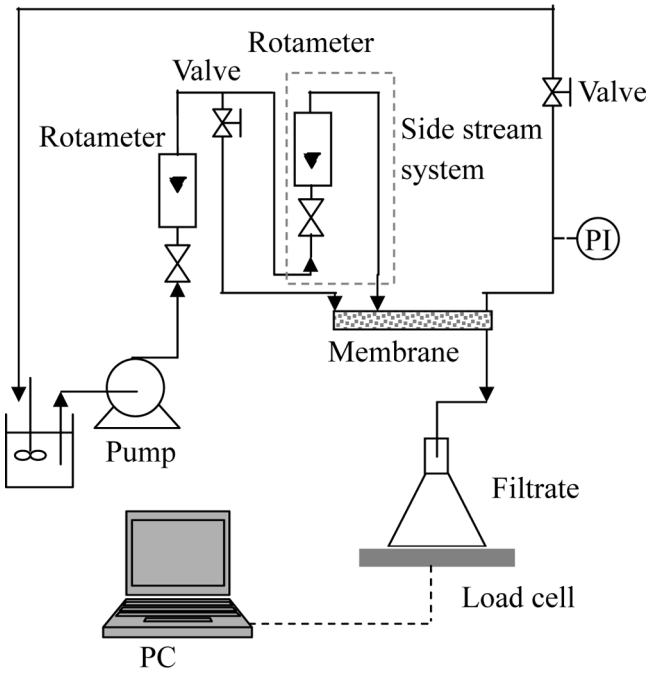

FIG. 1. The flow chart of cross-flow microfiltration with side stream system.

The transmission pump (Masterflex® model 7518-00) is switched on, and the suspension fluid is conveyed to the filtration chamber through the circulation system. The Rotameters are adjusted to control the main cross-flow and side stream speed in the filtration chamber. The suspension fluid passes through the filtration chamber and the needle valve before returning to the original suspension fluid vessel. The needle valve is adjusted to control the backflow volume and control the pressure differential. The weight of the filtered fluid which passed through the filtration chamber and the filter membrane is calculated in the collection container by an electronic balance (Precisa BJ 8100D). The electronic balance is connected to a personal computer; the computer will automatically record the weight data on the electronic balance. After filtering for a certain period of time and waiting for the filtrate flux to become stable, the experiment can be stopped. The filtrate can be extracted for further analysis, or the filter cake on the device's filter membrane can be removed for weighing (Precisa XS 225A) and drying.

In addition, the experiment utilized a parallel panel cross-flow microfiltration device with side stream. A top view of the sketch map of the side stream cross-flow filtration basic system is shown in Fig. 2. The cross-flow filtration module is composed of two acrylic panels; the filtration chamber is composed of silicone gaskets with a thickness of 3×10^{-3} m, a length of 5.5×10^{-2} m, and a width of 2.0×10^{-2} m. The filtration area is $1.1 \times 10^{-3}\,m^2$. Due to changes in the flow strength on the membrane, the production of the filter cake will be impacted. In this study, we attempted to alter the flow strength on the surface membrane to increase the shear force on the membrane and reduce the production of filter caking. As a result, the basic construction of the original cross-flow filter was improved; another channel was added to the side of

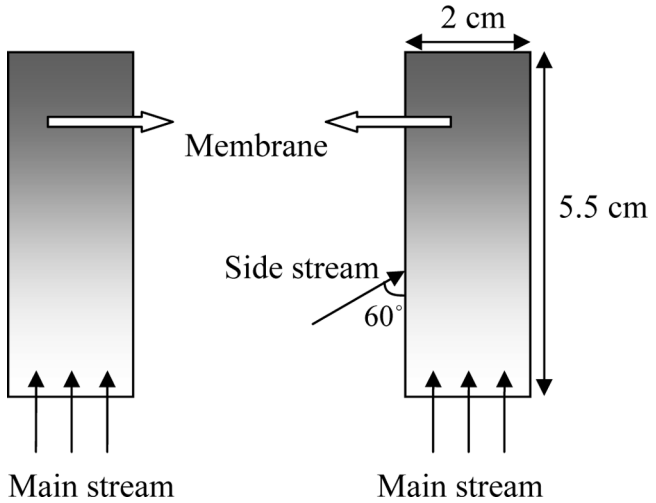

FIG. 2. Top view of membrane and side stream.

the original chamber. This side channel was introduced to the chamber at a 60° angle, as shown in Fig. 2.

Also, proportions of the filtration chamber are identical to those of the basic construction; the filtration area remains $1.1 \times 10^{-3}\,m^2$. Only a channel entrance has been added to the side; the cross-sectional area is $3 \times 10^{-6}\,m^2$, the entrance is at one-third of the main stream. The experimental process is largely similar to that of the basic apparatus, with the exception that the single channel has been divided into a two channel to make the same energy loss (with a single pump as the source of the driving force).

GOVERNING EQUATIONS AND BOUNDARY CONDITIONS

Figure 3 depicts the calculation logic, the upper flow channel, the central membrane, the bottom outflow, and the boundary conditions.

For the Newtonian fluid flow in the flow channel, the governing equation is the steady-state Navier-Stokes equation, which can be stated as follows:

$$\left(\vec{u}_f^{\,*} \bullet \nabla\right)\vec{u}_f^{\,*} + Eu\nabla P^* = \frac{1}{\mathrm{Re}}\nabla^2\vec{u}_f^{\,*}, \tag{1}$$

where $\vec{u}_f$ is the mainstream velocity. The first and the second terms of the left-hand-side of Eq. (1) correspond to the inertial and pressure effect, respectively; while the right-hand-sides corresponds to the viscous effect.

The governing equation for the fluid velocity $\vec{u}_p$ within the porous membrane taking into account the viscous effect is stated as follows:

$$\mathrm{Re}\,\vec{u}_p^{\,*2} = -\beta^2\vec{u}_p^{\,*} - Eu\mathrm{Re}\,\nabla P^*, \tag{2}$$

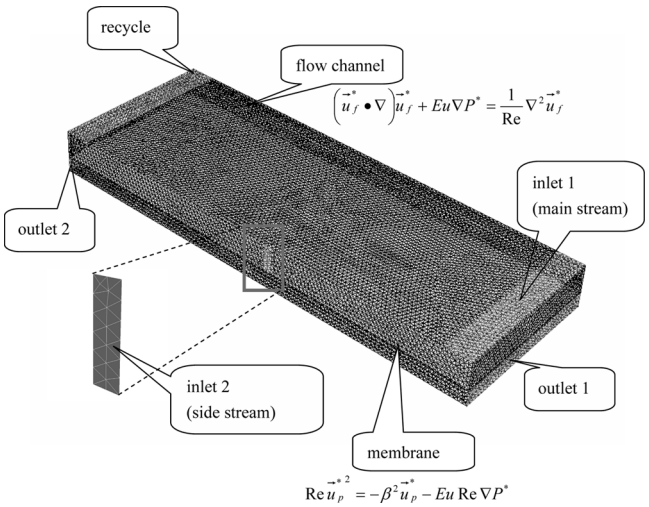

FIG. 3. Overall meshes in simulation and governing equations.

where $\mathrm{Re} = d_f\rho V/2$ (Reynolds number), $Eu = P_0/\rho V^2$ (Euler number), $\beta = d_f/2k^{0.5}$, $P^* = p/P_0$ and $\vec{u}_p^{\,*} = \vec{u}_p/V$. The two terms in the right-hand-side of Eq. (2) is the Darcy's law. The left-hand-side is attributed to the momentum sink, a modification version of Darcy's law.

The boundary conditions are as follows:

$$\vec{u}_f = v, \quad @ \text{ inlet 1 and inlet 2} \tag{3a}$$
$$\vec{u}_f = v_{recycle}, \quad @ \text{ recycle} \tag{3b}$$
$$P = 0, \quad @ \text{ outlet 1 and outlet 2} \tag{3c}$$
$$\vec{u}_p = \vec{u}_f, \quad @ \text{ membrane's surface} \tag{3d}$$
$$\nabla\vec{u}_p = \nabla\vec{u}_f, \quad @ \text{ membrane's surface} \tag{3e}$$

Equation (3a) states that the cross-flow velocity (main stream and side stream) is moving at a constant speed, while Eq. (3b) states that the recycle velocity is $v_{recycle}$, according to the experiment. Equation (3c) describes that the outlet pressure is atmospheric pressure. Equations (3d) and (3e) are the continuation conditions of fluid velocity and shear stress across the surface of membrane.

The computational fluid dynamics program FLUENT 6.1 (Fluent Inc., USA) solved the governing equations, Eqs. (1) and (2), together with the associated boundary conditions Eqs. (3a)–(3e), using construted mesh volumes. The numbers of the mesh volumes in the fluid side and within the porous membrane are about 250,000 and 50,000, respectively. The calculations were carried out with a maximum relative error of 10^{-4} in fluid velocity evaluation.

RESULTS AND DISCUSSION

Cross-Flow Filtration

Figure 4 is a diagram depicting the relationship between the filtration rate q and the filtration time t under different pressures and suspension fluid concentrations. The solid, open, and the dotted symbol each represent pressure differential values of 25, 50, and 75 kPa, respectively. The circles, squares, and triangles represent concentrations of 0.1, 0.2, and 0.3%, respectively. It can be seen from Fig. 4 that the greater the pressure difference is, the higher the filtrate flux will be; however, a longer time is required for reaching a stable filtration rate (under 25 and 50 kPa, the time needed for reaching a stable filtrate flux is approximately 1000–2000 seconds, while the time needed for reaching a stable filtrate flux under 75 kPa is approximately 3000–4000 seconds). This is a result of particles moving out of place due to squeezing and leading to longer stabilization times for the filtrate flux under higher pressure. In addition, under various pressures, the filtration rate will be higher with lower concentration.

Figure 5 depicts the total resistance values corresponding to the achievement of stable filtrate flux as calculated

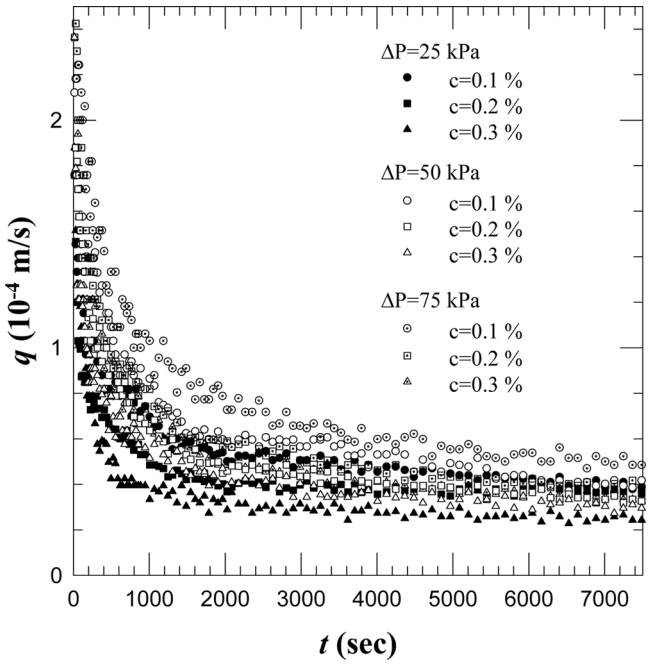

FIG. 4. Permeate flux versus time.

using Eq. (4) under different pressures.

$$q = \frac{\Delta P}{\mu R_t} \tag{4}$$

From Fig. 5 it can be seen that membrane resistance increases along with increases in pressure and concentration.

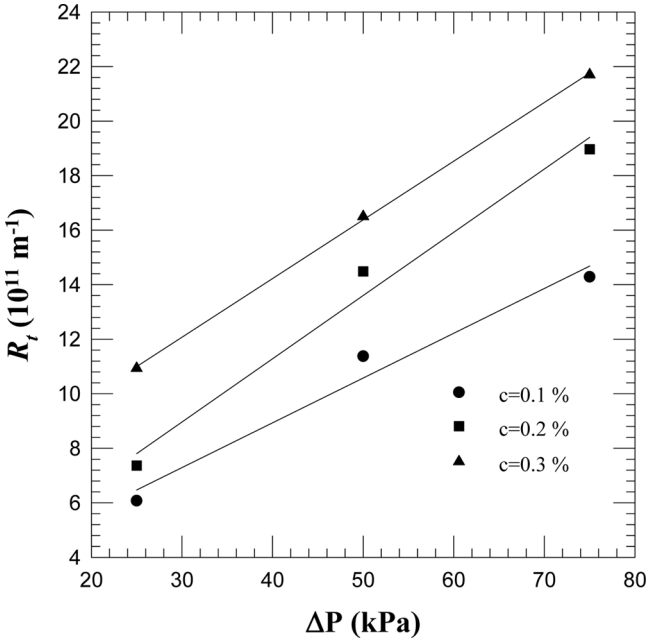

FIG. 5. Overall resistance versus pressure difference.

Cross-Flow Filtration with Side Stream

Figure 6 depicts the cake volume on the membrane surfaces under different side stream flow volumes. Of the two sets of numbers within the parentheses, the first represents the mainstream mass flow rate, while the second represents the side stream mass flow rate. Figures 6a and 6e depict typical cross-flow filtration (mass flow rate- = 6 g/s, 12 g/s). Figures 6b to 6d depict increases in the side stream flow rate, from 0.6 g/s, 3 g/s, to 6 g/s. It can be seen that when the mass flow of the side stream increases, shear

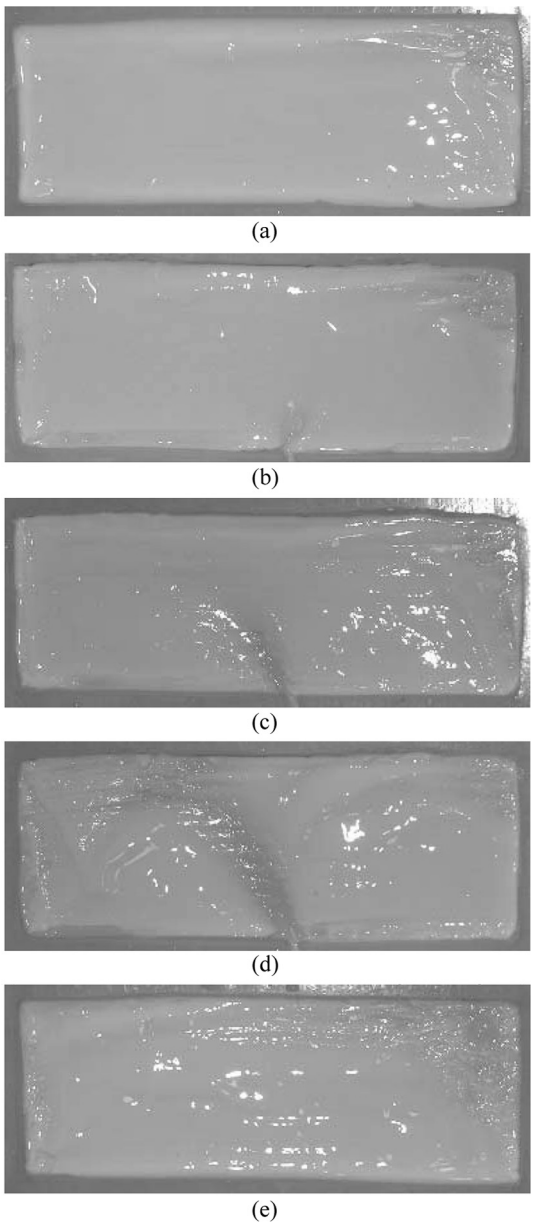

FIG. 6. Photograph of wet cake (ΔP = 50 kPa, C = 0.2 wt%) (a) v = 0.1 m/sec (6 g/sec) (b) v = 0.1 m/sec (6 g/sec: 0.6 g/sec) (c) v = 0.1 m/sec (6 g/sec: 3 g/sec) (d) v = 0.1 m/sec (6 g/sec: 6 g/sec) (e) v = 0.2 m/sec (12 g/sec).

force also increases and can carry away particles accumulated on the membrane surface, creating a clear side stream channel. There is no obvious accumulation of particles in this channel; as a result, the filtration resistance of the membrane as a whole decreases and the filtrate flux increases.

Figures 7a–7c depict changes in total resistance R_t along with time under the pressures of 25, 50, and 75 kPa, different mass flow of the side stream, and with concentration under 0.2%. With Fig. 7b as an example, it can be seen that resistance is reduced as long as there is a side stream. This is a matter of course, as shear force increases along with total volumetric flow rate. More worthy of note are the solid diamond and the solid inverted triangle data. The total flow rate is 12 g/s in all cases. However, if the total flow rate is split into a main stream of 6 g/s and a side stream of 6 g/s, then the total resistance is decreased by approximately 15% under stable filtrate flux. This demonstrates that appropriate introduction of a side stream is of aid in increasing the filtrate flux as long as the same pump acts as the driving force for conveying the suspension fluid.

Figures 8a–8c depict the relationships between pressure and stable filtrate flux q_s, dry filter cake weight W_c, and stable filtrate flux total resistance R_t under a different mass flow of the side stream. From these figures it can be seen that increasing the mass flow of the side stream increases the stable filtrate flux, while the dry cake weight and total resistance values decrease.

Simulation of Shear Force on Membrane

As mentioned, shear force is an important factor affecting particles depositing on the membrane surface. In this study it is calculated as:

$$F_t = \int_0^H \int_0^W \left[\left(-2\mu\frac{\partial v_x}{\partial x} + \frac{2}{3}\mu(\nabla \cdot v)\right)\right] dy\, dz + \int_0^W \int_0^L \left[-\mu\left(\frac{\partial v_x}{\partial y} + \frac{\partial v_y}{\partial x}\right)\right] dx\, dy + \int_0^L \int_0^H \left[-\mu\left(\frac{\partial v_z}{\partial x} + \frac{\partial v_x}{\partial z}\right)\right] dz\, dx \quad (5)$$

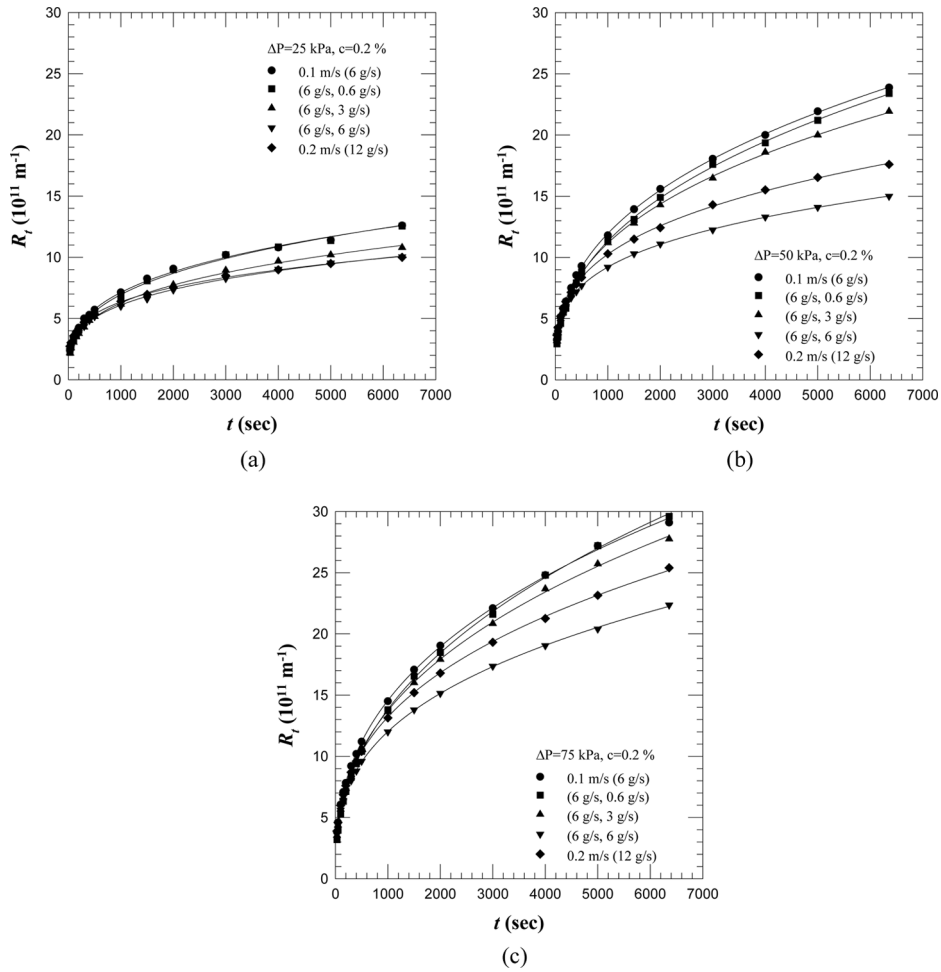

FIG. 7. Overall resistance during filtration (C = 0.2 wt%) (a) ΔP = 25 kPa (b) ΔP = 50 kPa (c) ΔP = 75 kPa.

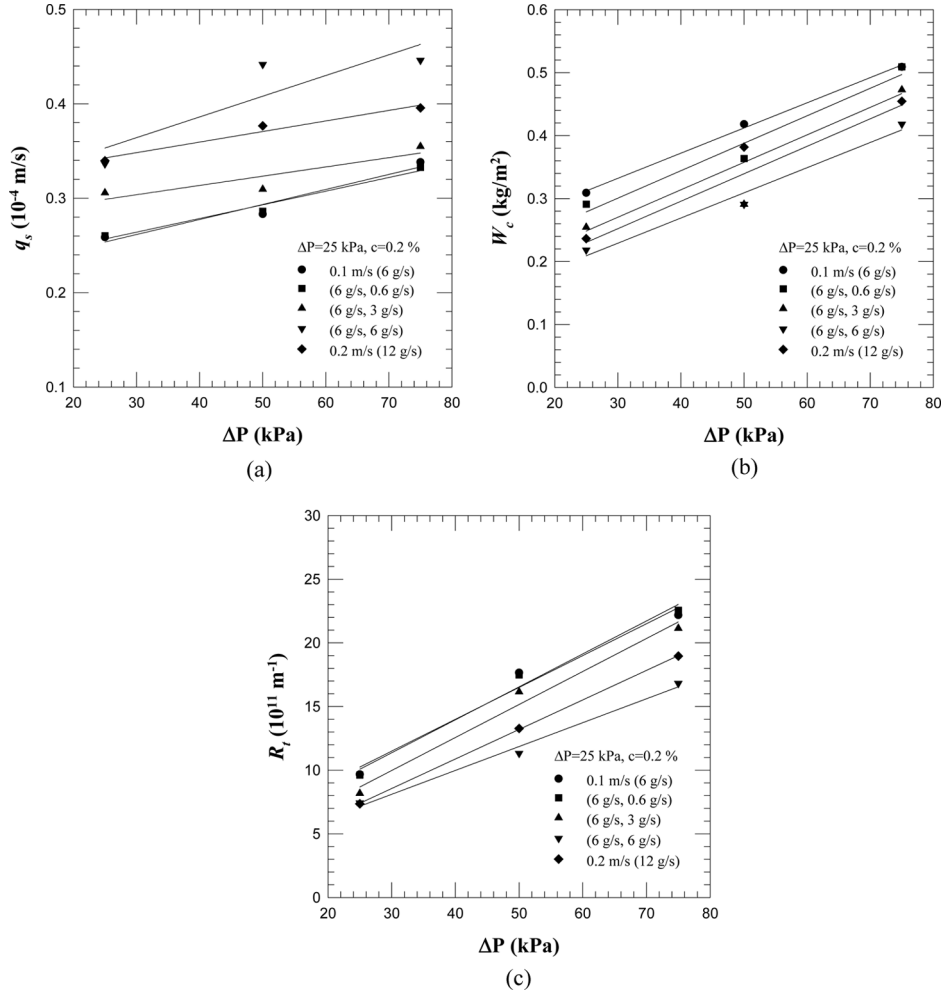

FIG. 8. Characteristics of filtration variances versus pressure (a) stable filtration rate (b) dry cake weight (c) total resistance.

Figure 9 is a diagram depicting the shear force on the membrane surface along the flow direction obtained through CFD calculation. Solid circles and solid diamonds depict shear force on the membrane surface with flow rates of 6 g/s and 12 g/s, respectively, under circumstances in which there is no side stream. The total filtration channel is 0.55 m; due to the end effect, only the force impacts of 0.01–0.05 m are shown. With a main stream flow rate of 12 g/s as an example, the 0.00015 N at 0.01 m is quickly reduced to 0.0001 N at 0.02 m. Thereafter, the shear force values of the membrane are fixed, meaning that, with the main stream filtration, the shear force experienced by the front end is greater; the shear force received thereafter is maintained at about a fixed value. This study introduced a side stream around where shear force was maintained at a fixed value, or at 0.18 m. Figure 9 shows that when the side stream enters the flow channel, the shear force experienced by the membrane surface increases, aiding in slowing the formation of filter cake. At approximately

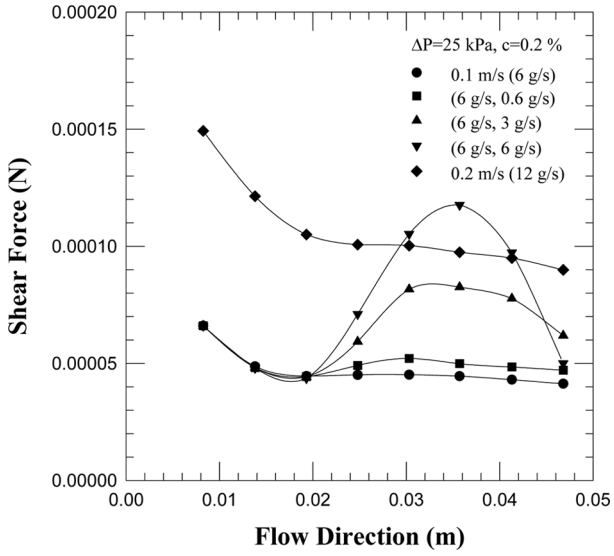

FIG. 9. Calculated shear force along flow direction.

0.035 m, the shear force begins to decrease again as a result of the side stream beginning to collide with the lateral wall, causing the flow to not simply continue forward; some back flow may occur. The above results show that, with identical energy loss (with a single pump as the source of driving force), the introduction of a side stream can effectively increase the membrane shear force, slowing the formation of the filter cake and reducing the total filter resistance and thus increasing the filtrate flux.

CONCLUSIONS

This work studied cross-flow filtration w/o a side stream from experiments and simulation. With identical energy loss, the introduction of a side stream can effectively increase membrane shear force, decreasing the formation of the filter cake and reducing the total filter resistance and thus increasing the filtrate flux. Further work should investigate the optimization of the side stream flow rate, the number of side streams introduced, as well as the speed and angle of the introduced side streams.

NOMENCLATURE

d_f	particle diameter (m)
Eu	Euler number (-)
F_t	shear force on membrane surface (N)
k	permeability of membrane (m^2)
P	pressure (N/m^2)
q	filtrate rate (m/s)
q_s	stable filtrate rate (m/s)
F_D	drag force, N
Re	Reynolds number (-)
R_t	total filtration resistance (m^{-1})
u_f	velocity in flow channel (m/s)
u_p	velocity in membrane (m/s)
W_c	weight of cake (kg/m^2)

Greek Letters

β	dimensionless permeability of membrane (-)
μ	viscosity of fluid (kg/m-s)
ρ	density of fluid (kg/m^3)

ACKNOWLEDGEMENTS

The authors would like to thank the National Science Council of the Republic of China, Taiwan, for financially supporting this research under Contract No. NSC 95-2214-032-051.

REFERENCES

1. Hwang, K.J.; Lin, K.P. (2002) Cross-flow microfiltration of dual-sized submicron particles. *Sep. Sci. Technol.*, 37 (10): 2231–2249.
2. Hwang, K.J.; Chang, Y.C. (2004) The use of cross-flow microfiltration in purification of liposomes. *Sep. Sci. Technol.*, 39 (11): 2557–2576.
3. Hwang, K.J.; Hsieh, Y.T.; Wang, W.T. (2006) Cross-flow microfiltration of fine particles suspended in polymeric aqueous solution. *Sep. Sci. Technol.*, 41 (8): 1551–1563.
4. Datta, S.; Gaddis, J.L. (1997) Dynamics and rheology of fouling cakes formed during ultrafiltration. *Sep. Sci. Technol.*, 32 (1–4): 327–353.
5. Ndinisa, N.V.; Fang, A.G.; Wiley, D.E.; Fletchwe, D.F. (2006) Fouling control in a submerged flat sheet membrane system: Part II – two-phase flow characterization and CFD simulations. *Sep. Sci. Technol.*, 41 (7): 1411–1445.
6. Hwang, K.J.; Chen, F.F. (2007) Modeling of particle fouling and membrane blocking in submerged membrane filtration. *Sep. Sci. Technol.*, 42 (12): 2595–2614.
7. Tung, K.L.; Shiau, J.S.; Chuang, C.J.; Li, Y.L.; Lu, W.M. (2002) CFD analysis on fluid flow through multifilament woven filter cloths. *Sep. Sci. Technol.*, 37 (4): 799–821.
8. Peng, M.; Vane, L.M.; Liu, S.X. (2004) Numerical simulation of concentration polarization in a pervaporation module. *Sep. Sci. Technol.*, 39 (6): 1239–1257.
9. Okada, H.; Mitsuhashi, K.; Ohara, T.; Whitby, E.R.; Wada, H. (2005) Computational fluid dynamics simulation of high gradient magnetic separation. *Sep. Sci. Technol.*, 40 (7): 1567–1584.
10. Wardle, K.E.; Allen, T.R.; Swaney, R. (2006) Computational fluid dynamics (CFD) study of the flow in an annular centrifugal contactor. *Sep. Sci. Technol.*, 41 (10): 2225–2244.
11. Wardle, K.E.; Allen, T.R.; Swaney, R. (2009) CFD simulation of the separation zone of an annular centrifugal contactor. *Sep. Sci. Technol.*, 44 (3): 517–542.
12. Berman, A.S. (1953) Laminar flow in channels with porous walls. *J. Appl. Phys.*, 24 (11): 1232–1235.
13. Deen, W.M. (1987) Hindered transport of large molecules in liquid-filled pores. *A.I.Ch.E. J.*, 33 (9): 1409–1425.
14. Drew, D.A.; Schonberg, J.A.; Belfort, G. (1991) Lateral inertial migration of a small sphere in fast laminar flow through a membrane duct. *Chem. Eng. Sci.*, 46 (12): 3219–3224.
15. Hwang, K.J.; Chang, D.J.; Hsu, F.C. (1995) Steady-state permeate flux of cross-flow microfiltration. *J. Membr. Sci.*, 98 (1–2): 97–106.
16. Bowen, W.R.; Sharif, A.O. (1998) Hydrodynamic and colloidal interactions effects on the rejection of a particle larger than a pore in microfiltration and ultrafiltration membranes. *Chem. Eng. Sci.*, 53 (5): 879–890.
17. Gupta, B.B.; Howell, J.A.; Wu, D.; Field, R.W. (1995) A helical baffle for cross-flow microfiltration. *J. Membr. Sci.*, 99 (1): 31–42.
18. Millward, H.R.; Bellhouse, B.J.; Sobey, I.J.; Lewis, R.W.H. (1995) Enhancement of plasma filtration using the concept of the vortex wave. *J. Membr. Sci.*, 100 (2): 121–129.
19. Ma, H.; Bowman, C.N.; Davis, R.H. (2000) Membrane fouling reduction by backpulsing and surface modification. *J. Membr. Sci.*, 173 (2): 191–200.
20. Kuberkar, V.T.; Davis, R.H. (2001) Microfiltration of protein-cell mixtures with crossflushing or backflushing. *J. Membr. Sci.*, 183 (1): 1–14.
21. Hoek, E.M.V.; Kim, A.S.; Elimelech, M. (2002) Influence of cross-flow membrane filter geometry and shear rate on colloid fouling in reverse osmosis and nanofiltration separations. *Environmental Eng. Sci.*, 19 (6): 357–372.
22. Jaganathan, S.; Tafreshi, H.V.; Pourdeyhimi, B. (2008) A case study of realistic two-scale modeling of water permeability in fibrous media. *Sep. Sci. Technol.*, 43 (8): 1901–1916.
23. Yang, W.J.; Wang, C.C.; Hsu, R.Y.; Wu, R.M. (2008) Two-phase flow simulation of reactor clarifiers. *J. Chinese Institute of Chemical Engineers*, 39 (3): 275–280.
24. Wu, R.M.; Lin, M.H.; Lin, H.Y.; Hsu, R.Y. (2006) 3D simulations of hydrodynamic drag forces on two porous spheres moving along their centerline. *J. Colloid Interface Sci.*, 301 (1): 227–235.
25. Hwang, K.J.; Wu, W.H.; Qian, S.; Nagase, Y. (2008) CFD study on the effect of hydrocyclone structure on the separation efficiency of fine particles. *Sep. Sci. Technol.*, 43 (15): 3777–3797.
26. Hsu, C.Y.; Wu, R.M. (2008) Hot zone in a hydrocyclone for particles escape from overflow. *Drying Tech.*, 26 (8): 1011–1017.